Journal of Colloid and Interface Science 478 (2016) 421–429

Contents lists available at ScienceDirect

Journal of Colloid and Interface Science

journal homepage: www.elsevier.com/locate/jcis

Regular Article

Three-dimensional honeycomb-like structured zero-valent iron/chitosan composite foams for effective removal of inorganic arsenic in water

Fengchao Su [a,b], Hongjian Zhou [b,*], Yunxia Zhang [b], Guozhong Wang [a,b,*]

[a] School of Physics and Materials Science, Anhui University, Hefei 230601, PR China
[b] Key Laboratory of Materials Physics, Centre for Environmental and Energy Nanomaterials, Anhui Key Laboratory of Nanomaterials and Nanotechnology, Institute of Solid State Physics, Chinese Academy of Sciences, Hefei 230031, PR China

GRAPHICAL ABSTRACT

The three dimensional honeycomb-like structured nanoscale zero-valent iron/chitosan composite foams were fabricated by a facile the freeze-drying method and exhibited excellent removal capability to As(III) and As(V) and avoided the secondary pollution of nanoscale zero-valent iron related species.

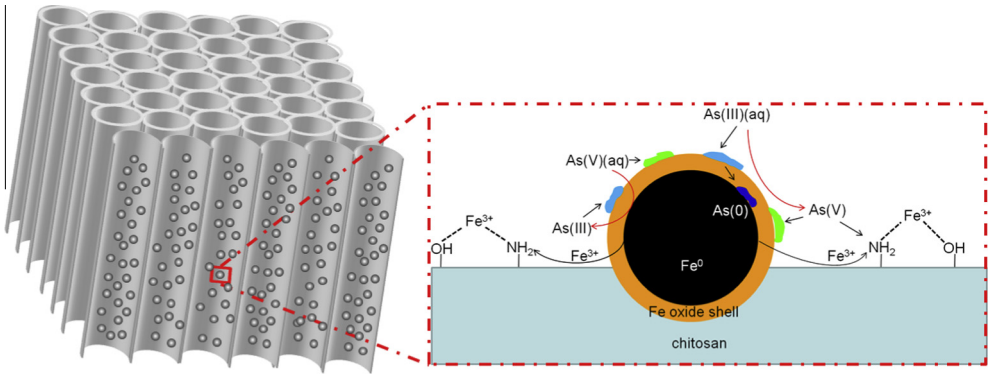

ARTICLE INFO

Article history:
Received 6 April 2016
Revised 13 June 2016
Accepted 13 June 2016
Available online 15 June 2016

Keywords:
Porous structure
Zero-valent iron
Inorganic arsenic
Secondary pollution
Chitosan composite

ABSTRACT

A facile freeze-drying method was presented to fabricate three dimensional (3D) honeycomb-like structured nanoscale zero-valent iron/chitosan composite foams (ICCFs) for effective removal of inorganic arsenic in water. It was found that freezing temperature has important influence on the formation of 3D network structure of ICCFs. The ICCFs obtained at freeze temperature of −80 °C exhibits oriented porous structure with good mechanical property than that at −20 °C, thus improved excellent removal capability of As(III) and As(V) up to 114.9 mg g^{-1} and 86.87 mg g^{-1}, respectively. Further, the adsorption kinetics of ICCFs on As(III) and As(V) can be described by pseudo-second order model and their adsorption isotherms follow Langmuir adsorption model. The superior removal performance of ICCFs on As(III) and As(V) can be ascribed to its oriented porous structure with abundant adsorption active sites resulted from nZVI and O, N-containing functional groups in ICCFs. Importantly, it was found that the O, N-containing functional groups of chitosan in ICCFs can adequately bind with the dissolved Fe^{3+} ions from oxidation of nZVI to form Fe^{3+}-Chitosan complex during removal of As(III) and As(V), thus effectively avoiding the dissolved Fe^{3+} ions into solution to produce secondary pollution. A possible

* Corresponding authors at: Institute of Solid State Physics, Chinese Academy of Sciences, Hefei 230031, PR China (H. Zhou and G. Wang).
E-mail addresses: hjzhou@issp.ac.cn (H. Zhou), gzhwang@issp.ac.cn (G. Wang).

http://dx.doi.org/10.1016/j.jcis.2016.06.035

adsorption-coupled reduction mechanism of ICCFs on As(III) and As(V) was also proposed based on the experimental results. We believe that this work would be helpful to develop low-cost and abundant chitosan-based materials as high performance adsorbents for environmental remediation applications.

1. Introduction

Arsenic contamination is notoriously known as one of the most harmful pollutants in surface and ground water, which has become a significant global environmental issue [1–3]. A high amount of arsenic in groundwater has been reported in Southeastern Asia, North and South America, and some parts of Europe [4,5]. Moreover, long term exposure to arsenic can cause serious health problems to human, such as keratosis, gangrene or cancer [6,7]. Inorganic arsenic in water environment can be present in two forms of nonionic trivalent arsenite [As(III)] complex and ionic pentavalent arsenate [As(V)] oxyanions, depending on the pH and redox potential of water environment [8]. Arsenic has been considered as the greatest health concern in some natural waters by the World Health Organization (WHO) [9]. Thus, it is still highly needed to develop a low-cost and highly efficient method to remove inorganic arsenic species from water environment.

Nanoscale zero-valent iron (nZVI) particles have been proved as a high efficient adsorbent to remove inorganic arsenic in water due to its high specific surface area and surface reactivity which is strongly depends on its particle size [10–12]. Although nZVI adsorbents directly applied to environmental remediation have demonstrated superior performance, the recycling and reusing of nZVI adsorbents are still very difficult owing to their small particle sizes and easy dissolution to form Fe^{3+} [8,13]. Some studies have revealed that highly concentrated residue of nZVI adsorbents and its released Fe^{3+} ions will bring secondary pollution to the environment and easily cause some potential adverse effects such as oxidative stress response, DNA and protein damage, mutagenic effects and cell death [14,15]. To solve this issue, a lot of efforts has been given to incorporate nZVI particles into porous substrates to improve the stability of nZVI in practical applications and effectively avoid the secondary pollution of nZVI-related species to environment, such as polymeric matrix [16], carboxymethyl cellulose [17], polyaniline [18], mesoporous silica [19], and pectin [20].

Chitosan has been widely used as substrate to construct composites with other nanomaterials because of its many advantages, such as low cost, wide availability, biodegradability, nontoxicity, and unique structural properties [21–23]. Importantly, chitosan possesses rich surface O- and N-containing functional groups such as —OH and —NH_2, very favourable for bonding transition metal ions through a chelation mechanism [24], and improve the removal efficiency of inorganic arsenic species from natural waters [25,26]. This may provide an effective means to construct nanostructured material (e.g., nZVI) incorporated chitosan composite for highly efficient removal of environmentally harmful substances, concurrently avoiding secondary pollution owing to the release of nanostructured material into environment.

Recently, the composite of nZVI particles incorporated into chitosan frameworks has been investigated and used as an adsorbent for removal of heavy metal ions, indicating superior removal performance compared to sole nZVI or chitosan as adsorbent. In this respect, Liu et al. synthesized chitosan beads supported nZVI as adsorbent to remove Cr(VI) in water, exhibiting great potential in practical applications [27]. Weng et al. reported a new material composed of bimetallic Fe/Ni nanoparticles incorporated into chitosan framework as adsorbent for removal of amoxicillin and Cd (II), demonstrating superior removal capability [28]. Liu et al. used epichlorohydrin/chitosan beads to immobilize nZVI particles for reduction of Cr(VI) from wastewater, displaying potential application in environmental remediation [29]. Horzum et al. fabricated chitosan fiber supported nZVI particles by liquid phase reduction approach using sodium borohydride for effective removal of arsenic [30]. Although the reported studies have demonstrated the benefits of chitosan as substrate to construct nanostructured material incorporated chitosan composites for high efficiency removal of environmentally harmful substances, the solid internal structure of chitosan obtained in the reported works by relatively complicated fabrication processes generally results in low removal capability toward environmentally harmful substances. Therefore, a simple way to design and development of chitosan-based composites with oriented porous structure as highly efficient adsorbents are still strongly desirable in the field of environmental remediation [23,31–33]. Recently, freeze-drying method has been widely used to fabricate porous materials with controllable pore structure, such as oriented porous structured inorganic, organic and their composite materials, exhibiting structure-dependent application performances [34–36].

In this work, three-dimensional (3D) honeycomb-like structured nZVIs/chitosan composite foams (ICCFs) were successfully fabricated by a facile freeze-drying method. The obtained ICCFs exhibits honeycomb-like porous structure with good mechanical stability, which has been characterized in detail by some characterization techniques such as SEM, elemental mapping analysis, XRD, FT-IR and stress testing. As an adsorbent for removal of As (III) and As(V) in water, the ICCFs demonstrates high removal capability due to its oriented porous structure which is favourable for mass transport of As-related species and fully contact with adsorption active sites of nZVI and O, N-containing functional groups in chitosan framework. Simultaneously, the experimental results also indicate that the Fe^{3+} ions resulted from oxidation of nZVI can be effectively bound with O, N-containing functional groups of chitosan to form Fe^{3+}-Chitosan complex, thus avoiding Fe^{3+} ions release into water to produce secondary pollution. Based on the experimental results, a removal mechanism of ICCFs on As(III) and As(V) has been proposed and discussed.

2. Experimental section

2.1. Materials

Iron sulfate heptahydrate ($Fe_2SO_4{\cdot}7H_2O$), acetic acid (CH_3-COOH), sodium arsenate, sodium arsenite and sodiumborohydride ($NaBH_4$) were purchased from the Sinopharm Chemical Reagent Co. Ltd. (Shanghai, China). Chitosan (deacetylation degree $\geqslant$75%, crystallinity index >0.57, 400 mpa s) was purchased from Aladdin Reagent Co. Ltd. (Shanghai, China). All chemicals were of analytical grade and used as received without further purification. Milli-Q water (18.2 MΩ cm^{-1}) was used throughout the whole experiments.

2.2. Preparation of 3D honeycomb-like structured nZVI/chitosan composite foams

An aqueous solution of 2.0 wt% chitosan was first prepared by dissolving 1.0 g chitosan into 49.0 mL of 0.1 mol L^{-1} acetic acid

solution. The above mixture was stirred at room temperature for 2 h to obtain a homogeneous chitosan solution. The nZVI, prepared as the reported method [37], was then added to the above chitosan solution to obtain a nZVI/chitosan mixture. For investigation of the effect of weight ratio of nZVI/chitosan on resulting composite structure, nZVI with different amounts (0.2 g, 0.4 g and 0.6 g) was added to the as-prepared chitosan solution under stirring vigorously to obtain nZVI/chitosan with weight ratio of 0.2 (0.2ICCF-80), 0.4 (0.4ICCF-80) and 0.6 (0.6ICCF-80).

The above obtained nZVI/chitosan solutions were further treated at −20 °C or −80 °C using a facile freeze-drying method as reported works [38]. Specifically, the nZVI/chitosan solution was placed into a plastic petri dish and rapidly transferred to a refrigerator at −20 °C (ICCF-20) or a deep freezer of −80 °C (ICCF-80) for 3 h to solidify the mixture. The frozen mixture was then transferred to a freeze dryer (SCIENTZ-18N, Ningbo Scieatz Biotechnology, China) at −80 °C and 1 pa for 36 h. To investigate the mechanical property of the ICCFs, the foam-type composite was then compressed into a flexible thin film at a pressure of 10 tons for 10 s using tablet machine. Remnant acetic acid was removed by soaking the ICCFs into enough solution of sodium borohydride. In addition, porous structured chitosan foams (CFs) were prepared at −20 °C (CF-20) and −80 °C (CF-80) as references using same method but without nZVI.

2.3. Characterization

Mechanical strength of the composites was measured using Instron Universal Tester (CMT 4204, SANS, China) at a crosshead speed of 5 mm/min and a span of 1 cm. Five 10 × 1.0 cm^2 rectangular pieces were measured, and the averaged result was adopted. The surface morphology of the composites was examined by field-emission scanning electron microscopy (FESEM, Quanta 200FEG, USA) at an acceleration voltage of 5 kV. The elemental distribution was analyzed by elemental mappings using FESEM operating at 15 kV. For the surface functional information, Fourier-transform infrared (FT-IR) spectrophotometer (JASCO, FTIR-410, Japan) was used in the region of 500–4000 cm^{-1}. The crystalline structures of composites were analyzed by X-ray diffraction (XRD, Philips, X'Pert-PRO, Netherlands) using $Cu_{K\alpha}$ radiation. The metal ion contents were determined by inductively coupled plasma optical emission spectrometer (ICP-OES, ICP-6300, Thermo Fisher Scientific, USA). The X-ray photoelectron spectroscopy (XPS) spectra of composites were recorded on an ESCALAB 250 X-ray photoelectron spectrometer (Thermo, America) equipped with Al $K\alpha_{1,2}$ monochromatized radiation at 1486.6 eV X-ray source.

2.4. Experiments for removal of As(III) and As(V)

Experiments were performed to evaluate the removal capability of ICCFs toward inorganic arsenic ions. In this study, sodium arsenate and sodium arsenite were used as the sources of the As(III) and As(V) ions, respectively. For the kinetic experiments, 50 mg ICCFs was added into 100 mL of As(III) or As(V) solution with initial arsenic concentration of 200 mg L^{-1} under stirring at 25 °C. Approximately 5.0 mL of solution was sampled from the suspension at certain time-interval between 0 min and 200 min. The sampled solution was then filtered quickly through a 0.22 μm membrane filter. The arsenic concentration in the sampled solution was determined by ICP-OES. The pH value in the reaction solution was maintained to be 6.0 ± 0.1 by 0.1 mol L^{-1} NaOH or 0.1 mol L^{-1} HCl. For the adsorption isotherms, the experiments were also carried out at pH 6.0 ± 0.1, and 50 mg ICCFs was added into 100 mL of arsenic solutions with different concentrations (0–250 mg L^{-1}) for 24 h. The influence of solution pH on removal performance of ICCFs (50 mg) was conducted within 100 mL of 200 mg L^{-1}As(III) and As(V) solution in a pH range of 4.0–9.0 for 24 h at 25 °C.

The removal capacity of the ICCFs for the arsenic ions was calculated according to the following equation (Eq. (1)):

$$q_e = \frac{V(C_0 - C_e)}{m} \quad (1)$$

C_0 is the initial arsenic ions in the solution (mg L^{-1}), C_e is the equilibrium concentration of arsenic ions after reaction with ICCFs (mg L^{-1}), V is the arsenic solution volume (L) and m is the mass of ICCFs (g).

3. Results and discussion

3.1. Structure and composition of ICCFs

Through a freeze-drying process, honeycomb-like structured ICCFs were fabricated using two pre-freezing samples as precursors at −20 °C (ICCF-20) and −80 °C (ICCF-80). In this process, the pore structure can be easily controlled by freezing temperature. Fig. 1 shows the surface and cross-sectional morphologies of ICCF-20 and ICCF-80, respectively. As shown, ICCF-80 exhibits uniformly arranged honeycomb-like porous structures in the sections perpendicular to the freezing direction compared to ICCF-20. Moreover, the pore distribution of ICCF-80 is more homogeneous than that of ICCF-20, approximately 120 μm (Fig. 1A and C). This can be due to a rapid ice crystallization of nZVI/chitosan suspension at −80 °C to induce the formation of oriented porous structure [39]. At −20 °C, ice growth rate was slower than that at −80 °C based on the reduced driving force for heat removal, even below the critical velocity for encapsulation of nZVI/Chitosan, thus resulting in large-sized ice crystals [38]. Hence, there was no preferred growth direction, likely due to the reduced temperature gradient, and nZVI/chitosan was expelled by ice fronts to form large, disoriented sheet like structures. Fig. 1B and D shows the cross-sectional views of ICCF-20 and ICCF-80 along the freezing direction. The pore channels in the ICCF-80 sample grew straight over the entire body, as shown in Fig. 1D, which indicates the ice crystals grew from the bottom (side of cooling medium) toward the upper surface of the gel body along the freezing direction. The mean thickness of the skeletal structure was approximately 15 μm, and the average channel size was 100 μm for ICCF-80. Each pore channel has repeating partitions with uniform spacing. The uniform and smaller porous structure in the composite foams freezed at −80 °C can greatly enhance mass transport, enabling contaminants fully contact with adsorption active sites provided by the entrapped nZVI particles and O, N-containing functional groups of chitosan in the composite.

The mechanical strength and removal capacity of ICCFs with different weight ratios of nZVI/Chitosan composites were investigated for removal of As(III) and As(V) ions, as shown in Fig. 2A and B. With increasing the ratios of nZVI/Chitosan, the mechanical strength of corresponding ICCFs was decreased from 13.13 MPa to 4.54 MPa. However, the removal capacity of ICCFs for As(III) and As(V) increases due to the nZVI with high weight ratio in ICCFs providing more adsorption active sites for As(III) and As(V). Considering the mechanical strength and removal capacity of ICCFs, the 0.4 wt ratio of nZVI/chitosan was chosen for the following experiments.

The influence of freezing temperature on mechanical property and removal capability of the ICCFs was also investigated, as shown in Fig. 2C and D. Under the freezing temperatures of −20 °C and −80 °C, the ICCF-20 and ICCF-80 exhibited an obvious different behavior in mechanical strength (Fig. 2C). The tensile strength of ICCF-80 was 11% higher than that of ICCF-20, and the

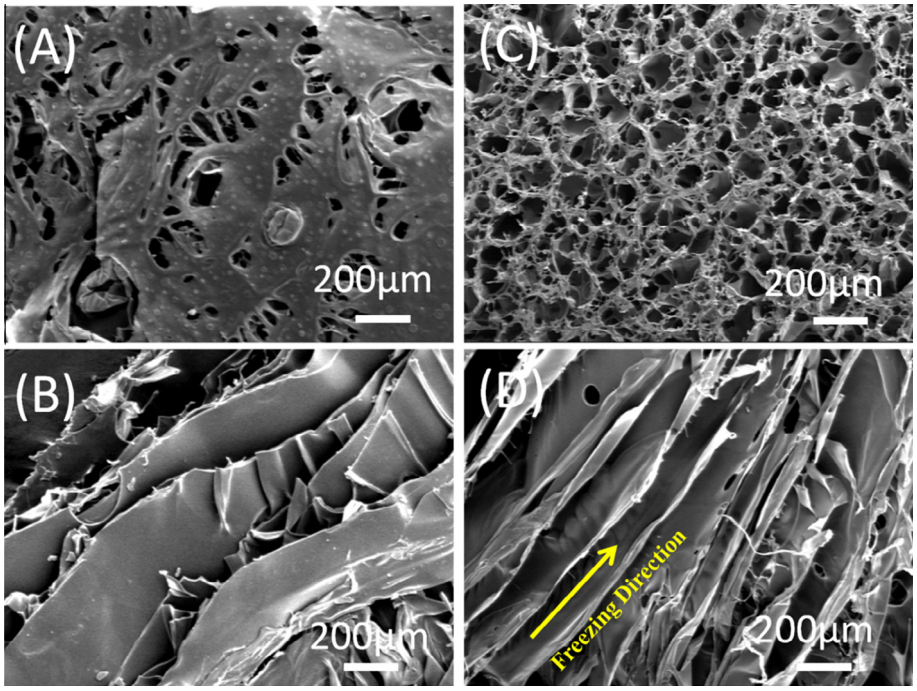

Fig. 1. The top view SEM micrograph of ICCF-20 (A) and ICCF-80 (C); the cross-sectional SEM micrograph of ICCF-20 (B) and (D) ICCF-80 along the freezing direction.

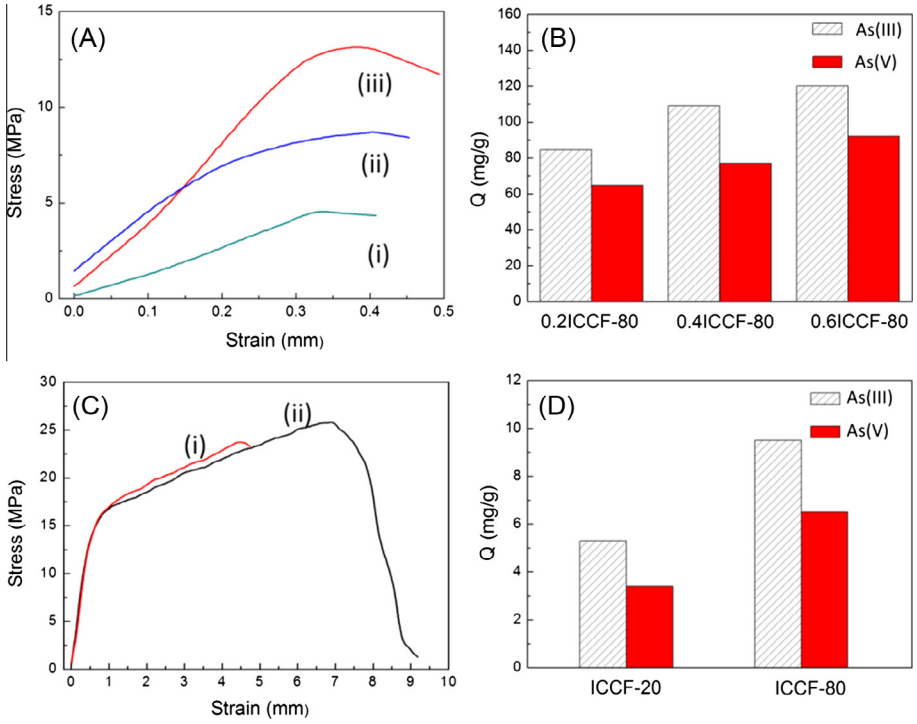

Fig. 2. (A) The mechanical property of 0.6ICCF-80 (i), 0.4ICCF-80 (ii) and 0.2ICCF-80 (iii); (B) the adsorption capacity of 0.2ICCF-80, 0.4ICCF-80 and 0.6ICCF-80 for As(III) and As(V); (C) the mechanical property of ICCF-20 (i) and ICCF-80 (ii); (D) the adsorption capacity of ICCF-20 and ICCF-80 for As(III) and As(V). Solution volume, solution concentration, shaking time, pH, sorbent amount and reaction temperature were 100 mL, 200 mg L^{-1} 24 h, pH 6.0, 50 mg, and 25 °C, respectively.

strain ratio of ICCF-20 film was less 40% lower than that of ICCF-80. For removal capability, 0.2 g of ICCF-80 or ICCF-20 was placed into 100 mL of As(III) or As(V) solution with 200 mg L^{-1}, respectively. From Fig. 2D, the removal amount of ICCF-20 toward As(III) and As(V) was 5.3 mg g^{-1} and 3.4 mg g^{-1}, however, ICCF-80 for As(III) and As(V) was 9.5 mg g^{-1} and 6.5 mg g^{-1}, respectively. Thus, the −80 °C of freezing temperature was used as the preparation condition in the following experiments.

Fig. 3 shows the SEM image and element mapping for the ICCF-80. The element mapping was employed to characterize the distribution of Fe, O and C in the ICCF-80. As shown in Fig. 3B –D, nZVI particles were dispersed homogenously into chitosan frameworks,

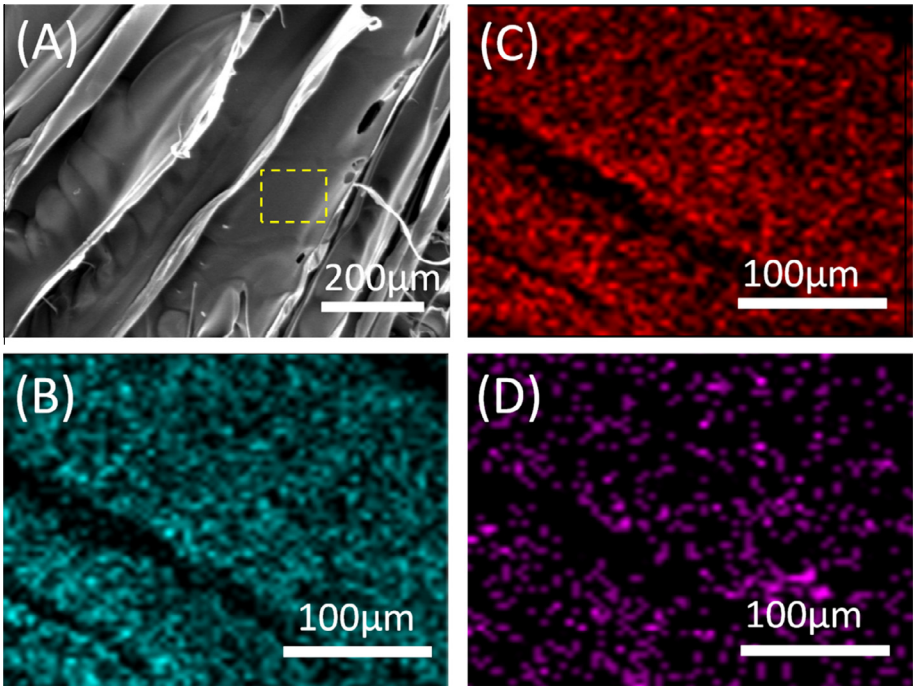

Fig. 3. (A) SEM image of ICCF-80 and elemental mapping images of (b) C, (c) O and (d) Fe from ICCF-80 due only to the dotted box of (A).

and the homogeneous distribution of C and O revealed the formation of chitosan backbone in the ICCF-80. Fig. S1A shows the XRD patterns of the as-prepared ICCF. The result (curve i) revealed the iron particles were existed in the ICCF-80. The typical diffraction peaks at 44.8°, 65.2°, and 82.5° can be indexed as the crystal planes (1 1 0), (2 0 0), (2 1 1) of nZVI phase (JCPDS NO. 01-087-0722). Fig. S1B presents the FTIR spectra of the ICCF-80 and chitosan, which identified the possible interactions between chitosan and nZVI particles. The spectrum of the chitosan (curve i in Fig. S1B) shows the characteristic peaks of chitosan at 3200–3500 cm^{-1} (O—H stretching and N—H stretching), 2920 and 2870 cm^{-1} (C—H stretching), 1600 cm^{-1} and 1580 cm^{-1} (C=O stretching in secondary amide), 1400 cm^{-1} (C—N stretching), 1073 cm^{-1} (C—O stretching). For the entrapment of nZVI particles in the chitosan foams, little shifts of the chitosan peaks were observed in the spectrum of ICCF-80 in Fig. S1B (curve ii). The results clearly revealed the interaction between nZVI and the O—H, C—N, and N—H groups of chitosan [30].

3.2. Removal capability of arsenic

The adsorption kinetic experiments for removal of As(III) and As (V) by ICCF-80 were carried out, as shown in Fig. 4A. It was clearly observed in Fig. 4A that the fast removal rates for As(III) and As(V) anions was occurred in the initial 40 min and achieved equilibrium in about 80 min and 120 min in the whole process, respectively. With increasing time, the removal amount of both As(III) and As (V) were gradually increased and the initial removal rates of As (III) was much higher than that of As(V). Around 80% and 48% of equilibrium removal amount were achieved for As(III) and As(V) within 20 min, respectively. To further understand the kinetics, the pseudo-second-order kinetic model was employed to describe the kinetic characteristics of the adsorption/reduction of As(III) and As(V) by the ICCF-80. The pseudo-second-order equation assumes that the rate of occupation of adsorption sites is proportional to the square of the number of unoccupied sites, expressed as follows (Eq. (2)):

$$\frac{t}{q_t} = \frac{1}{k_2 q_e^2} + \frac{t}{q_e} \tag{2}$$

where k_2 (g mg^{-1} min^{-1}) is pseudo-second-order rate constant. q_t and q_e reveal the adsorption capacity at time t and equilibrium, respectively. The values of the parameters q_e and k_2 for removal of As(III) and As(V) were estimated by non-linear fitting as listed in Table 1. The low values of k_2 indicate the removal rates of As(III) and As(V) were fast [28,40]. Furthermore,

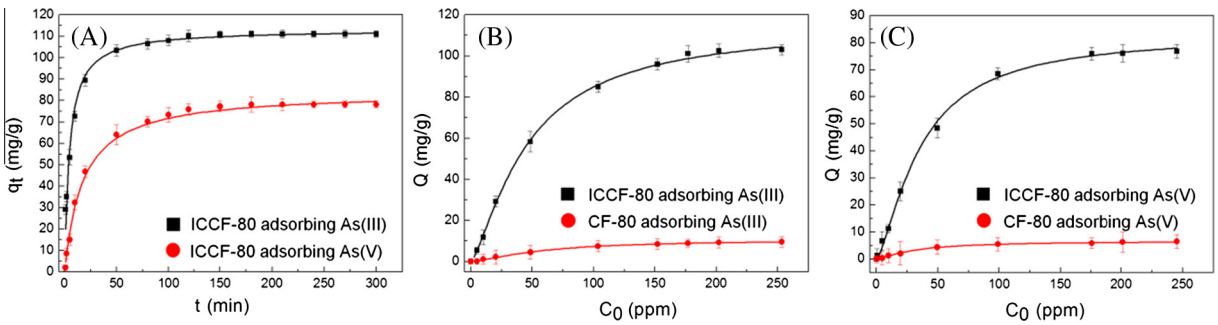

Fig. 4. (A) The kinetics curves of As(III) and As(V) on the ICCF-80; The isothermal adsorption of (B) As(III) and (C) As(V) on the ICCF-80 and CF-80. Solution volume, shaking time, pH, sorbent amount and reaction temperature were 100 mL, 24 h, pH 6.0, 50 mg, and 25 °C, respectively.

Table 1
Adsorption kinetic parameters obtained by pseudo-second-order model.

Arsenic	q_e (mg · g^{-1})	k_2 (g mg^{-1} min^{-1})	R^2	h (mg g^{-1} min^{-1})
As(III)	113.19	1.82×10^{-3}	0.990	23.32
As(V)	84.86	6.87×10^{-4}	0.996	4.95

nZVI/chitosan = 0.4, pH = 6.0, adsorption time = 10 h.

$h = k_2 q_e^2$ (mg g^{-1} min^{-1}) was calculated to quantitative describe of the initial removal rate from Eq. (1). The initial removal rate (h) of As(III) on the ICCF-80 was approximately five-fold higher than that of As(V), indicating removal of As(III) is much faster than that of As(V).

Based on the kinetic behavior, isothermal adsorption experiments were carried out on the removal of As(III) and As(V) by ICCF-80 and CF-80, as shown in Fig. 4B and C. With increasing initial concentration of arsenic from 1 to 120 mg L^{-1}, a gradual increased adsorption was observed. It has been found that the adsorption isotherms for both As(III) and As(V) on the ICCF and chitosan foams can be well described by Langmuir models, which is applicable for the monolayer adsorption on the surface containing a finite number of identical active sites.

The non-linear form of Langmuir isotherm model can be expressed as follows (Eq. (3)) [41]:

$$q_e = q_{\max} \frac{bc_e}{1 + bc_e} \tag{3}$$

Table 2
Parameters for Langmuir models of arsenic ions adsorption on ICCF-80 and CF-80.

Arsenic	q_{max} (mg g^{-1})		b (L mg^{-1})		R^2	
	ICCF-80	CF-80	ICCF-80	CF-80	ICCF-80	CF-80
As(III)	122.51	11.17	5.36×10^{-3}	4.33×10^{-3}	0.993	0.997
As(V)	84.48	6.87	7.71×10^{-3}	9.70×10^{-3}	0.998	0.996

where q_e, is the amount of arsenic ions adsorbed onto the ICCF per unit mass of ICCFs (mg/g) at equilibrium, C_e (mg/L) is the equilibrium concentration of arsenic ions in liquid phase, q_{max} (mg/g) is the theoretical maximum capacity of ICCFs for removal of arsenic ions. b (L/mg) denotes the Langmuir constants which is related to the adsorption-desorption energy and to the affinity of binding sites for arsenic ions.

Table 2 shows the calculated isotherm parameters along with correlation coefficients. Moreover, the maximum capacities q_{max} were up to 122.51 mg g^{-1} for As(III) removal and 84.48 mg g^{-1} for As(V) removal, while CF-80 have much lower capability as 11.17 mg g^{-1} and 6.87 mg g^{-1} for As(III) and As(V) removal, respectively. The Langmuir constants b of ICCF-80 is positive values, indicated the ICCFs is a favourable adsorbent. Such arsenic removal capacities are much higher than the most commercial adsorbents as well as the other nZVI/chitosan composites, as shown in Table S1 [30,42–50].

Inorganic arsenic in water can be present in the form of non-ionic trivalent arsenite [As(III)] complex and ionic pentavalent arsenate [As(V)] oxyanions, depending on the solution pH and redox potential [8]. Thus, the pH influence of arsenic solution on the removal capability of the ICCFs was investigated from pH 4.0 to 9.0 at the initial concentration of 200 mg L^{-1}, as shown in Fig. 5A and B. The equilibrium removal amount of As(III) is almost unchanged with pH value in the range of 4.0–7.0. While pH beyond 7.0, a significant decrease was observed in As(III) removal. For As (V) removal, the equilibrium removal amount decreases dramatically from 74.5 mg g^{-1} to 24.3 mg g^{-1} with increasing pH value from 4 to 9. According to the reports, the removal capacity of nZVI was decreased dramatically from 100% to 2.1% as the initial solution pH increased from 3.0 to 11.0, due to the precipitation of ferrous hydroxides on the surface of nZVI [51–53]. Compared with nZVI, the ICCFs have higher removal capability in the range of pH 4.0–7.0. The reason for the decreased removal amount of ICCFs for arsenic ions may be attributed to the repulsion by the

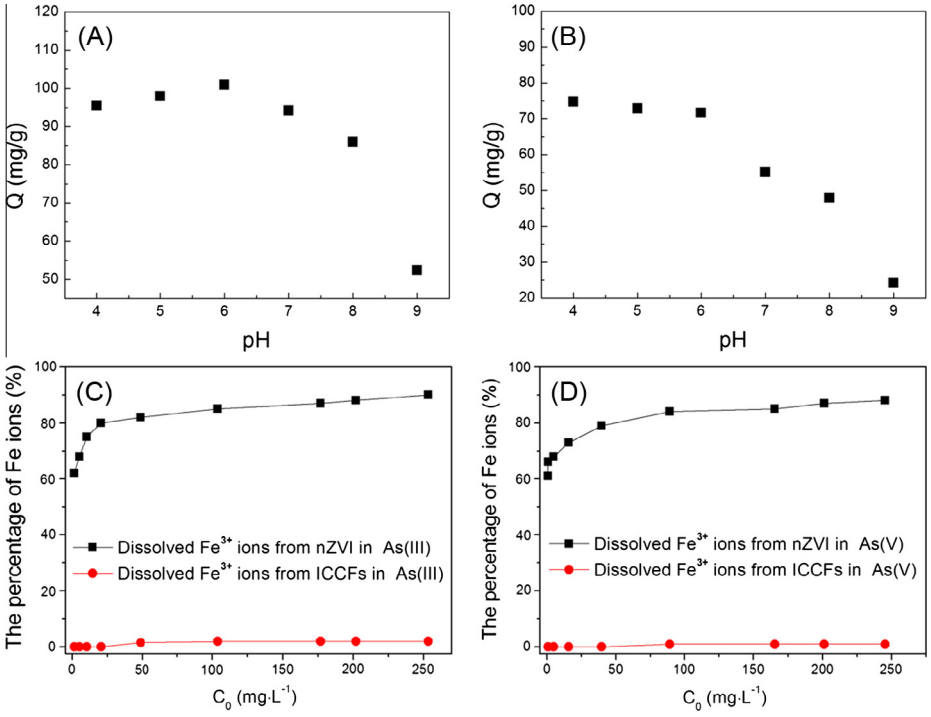

Fig. 5. Effect of pH on the sorption of (A) As(III) and (B) As(V) solutions by ICCFs; the percentage of dissolved Fe^{3+} ions from nZVI and ICCF-80 into the solution of (C) As(III) and (D) As(V). The initial concentration of arsenic ions is 200 mg L^{-1}.

negatively charged surface of ICCFs for the $H_2AsO_3^-$ (As(III)) and $H_2AsO_4^-/HAsO_4^{2-}$ ions (As(V)) in the alkaline conditions [30].

It has been reported that the release of highly concentrated nZVI-related species during environmental remediation may arouse adverse influence on aquatic environment [14,54]. Therefore, the iron dissolution of ICCFs was investigated in the arsenic treatment solution. Fig. 5C and D shows the percentage of Fe^{3+} ions dissolved into the arsenic solution from both ICCFs and nZVI with the increasing concentration of arsenic at pH 6.0. In Fig. 5C, with the increase of As(III) concentration, the percentage of dissolved Fe^{3+} ions from ICCFs into the solution increases gradually in the initial stage, and then achieved equilibration at 50 mg L^{-1} of initial arsenic concentration, while the concentration of dissolved Fe^{3+} ions from the nZVI has a sharp increase at low concentration of arsenic solution, and then remain gradually rising trend with increasing the concentration of arsenic ions. In Fig. 5D, a similar phenomenon can be observed for As(V). The maximum amount of dissolved Fe^{3+} ions from ICCFs was 1.9% and 0.9% for As(III) and As(V) respectively; while 90% and 88% of Fe^{3+} ions were released from nZVI to As(III) and As(V) solution respectively.

Many researchers have reported that chitosan has many functional groups on their backbone (e.g. amino groups and hydroxy groups), which is able to fix many transition metal ions by chelation. Therefore, it can be reasonably assumed that chitosan may bind with the dissolved Fe^{3+} ions from oxidation of nZVI in the ICCFs to further form Fe^{3+}-Chitosan complex, which could avoid the secondary pollution of nZVI. In order to prove the above hypothesis, we investigated the adsorption capability of chitosan foams for Fe^{3+} ions (see the Experimental section). From Fig. S2, we observed that both CF-20 and CF-80 have excellent adsorption capacity toward Fe^{3+} ions. Especially, the saturated adsorption capacity of CF-80 was 120 mg g^{-1}, because of 3D oriented porous structure of CF-80. Therefore, the oriented porous structured ICCFs have three advantages to avoid the secondary pollution of nZVI: (1) The ICCFs can be totally and easily separated from the solution, (2) the oxidized iron and iron ions were encapsulated in the chitosan; (3) the chitosan has a high adsorption capacity for Fe^{3+} ions [25,26,40].

3.3. The mechanism of arsenic removal by ICCFs

To verify the chemical reactions between arsenic and ICCFs, XPS was carried out to investigate the detailed information about the composition of ICCFs before and after reaction with arsenic solution. Fig. 6A shows the full scan XPS spectra of ICCFs before and after exposed to As(III) and As(V). For fresh ICCFs (the curve i in Fig. 6A), the sharp peaks in the full scan spectra revealed the presence of carbon, nitrogen, oxygen and iron elements at binding energies of 285, 530, 400, and 711 eV, respectively. The peaks of carbon and nitrogen were assigned to the chitosan and the oxygen peak originated from the oxide-layer of nZVI and O-containing functional groups of chitosan on the surface of ICCFs. After treated with As(III) and As(V), a new peak appeared at around 44 eV, indicating the uptake of arsenic on the surface of ICCFs (curve ii and iii in Fig. 6A).

The corresponding Fe 2p spectra of ICCFs before and after reacting with As(III) and As(V) solution were presented in Fig. 6B. The peaks at binding energies of 724.3 eV and 708.2 eV can be attributed to Fe_2O_3 and FeOOH, respectively, while the peaks at 711.9 eV and 725.8 eV can be regarded as the signals of Fe_3O_4 [51,53], indicating extensive oxidation of nZVI in ICCFs after adsorption of arsenic species. Furthermore, a feature peak of nZVI can be found at around 706.5 eV and 719.7 eV for $2p_{3/2}$ and $2p_{1/2}$, suggesting the existence of nZVI in ICCFs. After the reaction, the peak of nZVI could not be found and the peak intensity of nZVI and Fe^{3+} increased, indicating that an oxidation process of nZVI may occur. Moreover, the oxidized Fe^{3+} ions were bound with $—O^-$ and $—NH_2$ site of chitosan to form Fe^{3+}-Chitosan complex in the ICCFs, which not only avoid the secondary pollution of nZVI, but also enhance the removal capacity of nZVI-Chitosan composites. We also measured the XRD patterns of ICCFs before and after reacting with As (III) and As(V) ions. In Fig. S1A, a similar phenomenon was observed from XRD patterns of nZVI. The nZVI particles were oxidized to lepidocrocite (FeOOH) and magnetite (Fe_3O_4) after reaction with As(III) and As(V) ions.

Fig. 6C showed the XPS spectra of the sample reacted with As (III) and As(V). The reacted As(III) sample shows three peaks at 44.6, 43.4 and 40.6 eV, corresponding to As(V), As(III) and As^0, respectively [55]. Its demonstrated that only 34.3% of As(III) was found on the ICCFs surface. Meanwhile, 29.0% and 36.7% of As(III) was transfer to As(V) and As^0 by nZVI of ICCFs, indicating that both oxidation and reduction have occurred during the adsorption of As (III) by ICCFs. The concomitant observation of oxidation and reduction of As(III) by nZVI has been reported in previous study [52], and mentioned that nZVI exhibits broad functionality with the Fe^0 core having reduction capability and the hydroxide layer promoting oxidation and adsorption/co-precipitation. For reacted As(V) sample, 66.5% of As(V) ions were adsorbed onto the outer layer iron oxides of nZVI in the ICCFs, while 33.5% of As(V) were reduced by nZVI to As(III), as confirmed by XPS analysis. Adsorption of both As(III) and As(V) on the ICCFs occurs by forming inner-sphere complexes with the hydroxide shells of nZVI.

Overall, the proposed possible mechanism of adsorption-coupled reduction for As (III) and As(V) removal by ICCFs is presented in Fig. 7: The anionic $H_2AsO_3^-$ (As(III)) and $H_2AsO_4^-/HAsO_4^{2-}$ ions (As(V)) was first adsorbed onto the active sites of ICCFs by chelation or electrostatic attraction of protonated amine group in chitosan foams and nZVI particles. Next, the adsorbed arsenic ions

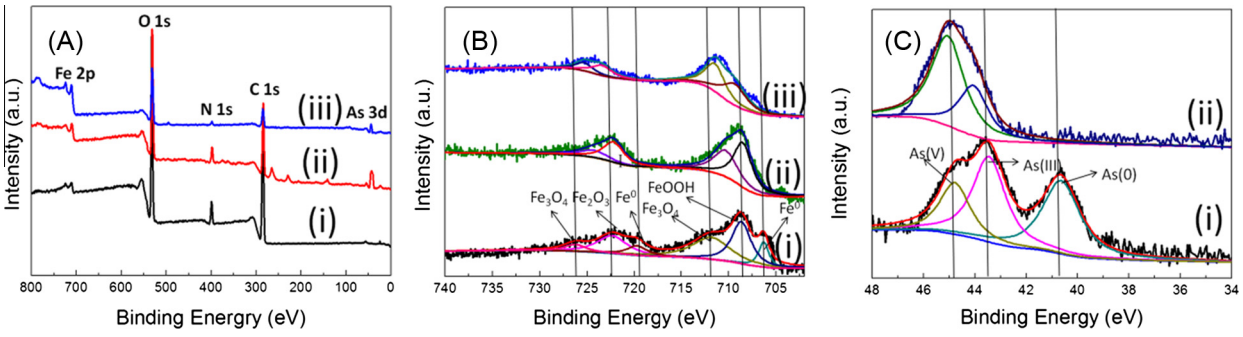

Fig. 6. (A) XPS survey of ICCFs before (curve i) and after reaction with 100 mg L^{-1} of As(III) (curve ii) and As(V) (curve iii) at pH 6.0; (B) XPS spectra of of Fe_{2p} before (curve i) and after reaction with 100 mg L^{-1} of As(III) (curve ii) and As(V) (curve iii) at pH 6.0; (C) XPS spectra of of As_{3d} after (curve i and ii) reaction with 100 mg L^{-1} of As(III) and As (V) at pH 6.0.

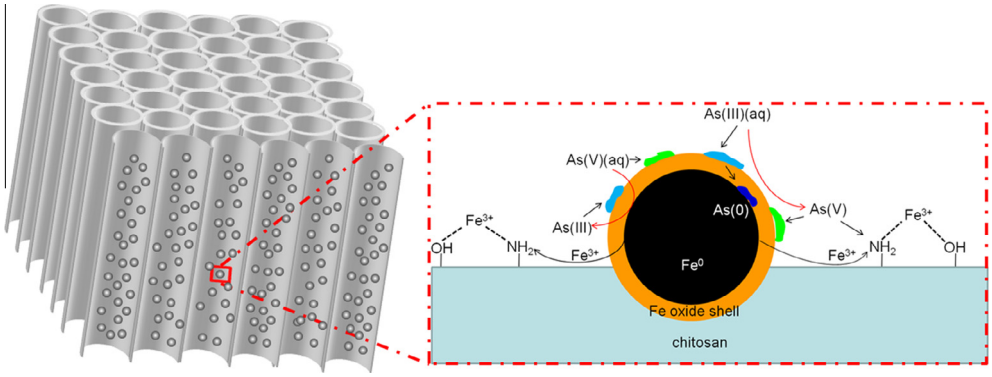

Fig. 7. Schematic representation of mechanistic pathway for arsenic removal by ICCFs.

were partially reduced by the adjacent nZVI. Afterwards, the oxidized Fe^{3+} ions of nZVI were in situ bound with —O^- and —NH_2 sites of chitosan to form Fe^{3+}-Chitosan complex in the ICCFs. Meanwhile, the formed Fe^{3+}-Chitosan complex created new active site to adsorb arsenic ions and thus enhanced the removal capacity of nZVI-chitosan composites [25,26,40,42,44]. Moreover, the unreacted As(V) and reduced As(III) and As^0 were all adsorbed on the ICCFs.

4. Conclusion

In summary, three dimensional oriented porous structured nZVI/chitosan composite foams have been successfully fabricated by a facile freeze-drying method. The formed oriented porous structure of ICCFs with good mechanical stability is favourable for promoting mass transport, thus improving the contaminant removal efficiency when used as adsorbents. The experimental results demonstrated that the obtained ICCFs at −80 °C as adsorbent exhibits excellent removal capability toward As(III) and As(V) up to 114.9 mg g^{-1} and 86.87 mg g^{-1} respectively, which was superior to most reported studies in literatures [30,42–48,50]. Importantly, it has been revealed that such porous structured chitosan could bind with the dissolved Fe^{3+} ions from oxidation of nZVI in the ICCFs to form Fe^{3+}-Chitosan complex, which avoids the secondary pollution of nZVI-related species. The possible mechanism of adsorption-coupled reduction was proposed for As(III) and As(V) removal by ICCFs. This study not only deepens the understanding of arsenic adsorption behaviors but also provides a promising and highly efficient arsenic adsorbent.

Acknowledgments

This work was supported by the National Basic Research Program of China (Grant No. 2013CB934302), the Natural Science Foundation of China (Grant Nos. 51472246, 21177132 and 51502296).

Appendix A. Supplementary material

Supplementary data associated with this article can be found, in the online version, at http://dx.doi.org/10.1016/j.jcis.2016.06.035.

References

[1] I. Ali, Chem. Rev. 112 (2012) 5073.
[2] I. Ali, Sep. Purif. Rev. 43 (2014) 175.
[3] K. Pan, W.X. Wang, Sci. Total Environ. 421 (2012) 3.
[4] L. Rodriguez-Lado, G. Sun, M. Berg, Q. Zhang, H. Xue, Q. Zheng, C.A. Johnson, Science 341 (2013) 866.
[5] N. Raychowdhury, A. Mukherjee, P. Bhattacharya, K. Johannesson, J. Bundschuh, G.B. Sifuentes, E. Nordberg, R.A. Martin, A. del Rosario Storniolo, J. Hydrol. 518 (2014) 300.
[6] K.S.M. Abdul, S.S. Jayasinghe, E.P. Chandana, C. Jayasumana, P.M.C. De Silva, Environ. Toxicol. Pharmacol. 40 (2015) 828.
[7] R. Singh, S. Singh, P. Parihar, V.P. Singh, S.M. Prasad, Ecotoxicol. Environ. Saf. 112 (2015) 247.
[8] Y. Yoon, W.K. Park, T.M. Hwang, D.H. Yoon, W.S. Yang, J.W. Kang, J. Hazard. Mater. 304 (2016) 196.
[9] I. Hojsak, C. Braegger, J. Bronsky, C. Campoy, V. Colomb, T. Decsi, M. Domellof, M. Fewtrell, N.F. Mis, W. Mihatsch, J. Pediatr. Gastroenterol. Nutr. 60 (2015) 142.
[10] F. Fu, D.D. Dionysiou, H. Liu, J. Hazard. Mater. 267 (2014) 194.
[11] S. Li, W. Wang, F. Liang, W.X. Zhang, J. Hazard. Mater. (2016), http://dx.doi.org/10.1016/j.jhazmat.2016.01.032.
[12] P. Huang, Z. Ye, W. Xie, Q. Chen, J. Li, Z. Xu, M. Yao, Water Res. 47 (2013) 4050.
[13] S. Bhowmick, S. Chakraborty, P. Mondal, W. Van Renterghem, S. Van den Berghe, G. Roman-Ross, D. Chatterjee, M. Iglesias, Chem. Eng. J. 243 (2014) 14.
[14] P.J. Chen, S.W. Tan, W.L. Wu, Environ. Sci. Technol. 46 (2012) 8431.
[15] P.J. Chen, W.L. Wu, K.C.-W. Wu, Water Res. 47 (2013) 3899.
[16] S. Xiao, M. Shen, R. Guo, S. Wang, X. Shi, J. Phys. Chem. C 113 (2009) 18062.
[17] C.M. Kocur, L. Lomheim, H.K. Boparai, A.I. Chowdhury, K.P. Weber, L.M. Austrins, E.A. Edwards, B.E. Sleep, D.M. O'Carroll, Environ. Sci. Technol. 49 (2015) 8648.
[18] B. Qiu, C. Xu, D. Sun, H. Yi, J. Guo, X. Zhang, H. Qu, M. Guerrero, X. Wang, N. Noel, ACS Sustainable Chem. Eng. 2 (2014) 2070.
[19] E. Petala, K. Dimos, A. Douvalis, T. Bakas, J. Tucek, R. Zboril, M.A. Karakassides, J. Hazard. Mater. 261 (2013) 295.
[20] D. Chen, K. Yang, H. Wang, J. Zhou, H. Zhang, RSC Adv. 5 (2015) 65068.
[21] T. Majima, T. Irie, N. Sawaguchi, T. Funakoshi, N. Iwasaki, K. Harada, A. Minami, S.I. Nishimura, Proc. Inst. Mech. Eng., Part H 221 (2007) 537.
[22] Y. Zhong, X. Song, Y. Li, Carbohydr. Polym. 84 (2011) 335.
[23] C. Liu, R. Bai, J. Membr. Sci. 279 (2006) 336.
[24] P. Miretzky, A.F. Cirelli, J. Hazard. Mater. 167 (2009) 10.
[25] R.N. Shinde, A.K. Pandey, R. Acharya, R. Guin, S.K. Das, N.S. Rajurkar, P.K. Pujari, Water Res. 47 (2013) 3497.
[26] J. Ma, Y. Shen, C. Shen, Y. Wen, W. Liu, Chem. Eng. J. 248 (2014) 98.
[27] T. Liu, X. Yang, Z.L. Wang, X. Yan, Water Res. 47 (2013) 6691.
[28] X. Weng, S. Lin, Y. Zhong, Z. Chen, Chem. Eng. J. 229 (2013) 27.
[29] T. Liu, Z.L. Wang, L. Zhao, X. Yang, Chem. Eng. J. 189 (2012) 196.
[30] N. Horzum, M.M. Demir, M. Nairat, T. Shahwan, RSC Adv. 3 (2013) 7828.
[31] L. Jiang, Z. Fan, Nanoscale 6 (2014) 1922.
[32] M.R. Awual, M.M. Hasan, Sens. Actuators, B 202 (2014) 395.
[33] M. Kumari, C.U. Pittman, D. Mohan, J. Colloid Interface Sci. 442 (2015) 120.
[34] M. Fukushima, Y.I. Yoshizawa, Mater. Lett. 153 (2015) 99.
[35] S. Han, D. Wu, S. Li, F. Zhang, X. Feng, Adv. Mater. 26 (2014) 849.
[36] U.G. Wegst, H. Bai, E. Saiz, A.P. Tomsia, R.O. Ritchie, Nat. Mater. 14 (2015) 23.
[37] E.J. Petersen, R.A. Pinto, X. Shi, Q. Huang, J. Hazard. Mater. 243 (2012) 73.
[38] F. Sun, B.K. Lim, S.C. Ryu, D. Lee, J. Lee, Mater. Sci. Eng., C 30 (2010) 789.
[39] J. Wu, J.C. Meredith, ACS Macro Lett. 3 (2014) 185.
[40] A.C. Zimmermann, A. Mecabo, T. Fagundes, C.A. Rodrigues, J. Hazard. Mater. 179 (2010) 192.
[41] Z. Aksu, Process Biochem. 38 (2002) 89.
[42] H.H. Santos, C.A. Demarchi, C.A. Rodrigues, J.M. Greneche, N. Nedelko, A. Slawska-Waniewska, Chemosphere 82 (2011) 278.
[43] B. Liu, D. Wang, H. Li, Y. Xu, L. Zhang, Desalination 272 (2011) 286.
[44] J.d. Marques Neto, C.R. Bellato, J.L. Milagres, K.D. Pessoa, E.S.d. Alvarenga, J. Braz. Chem. Soc. 24 (2013) 121.
[45] M.T. Sikder, S. Tanaka, T. Saito, M. Kurasaki, J. Environ. Chem. Eng. 2 (2014) 370.
[46] J. Wang, W. Xu, L. Chen, X. Huang, J. Liu, Chem. Eng. J. 251 (2014) 25.
[47] J. Qi, G. Zhang, H. Li, Bioresour. Technol. 193 (2015) 243.
[48] A. Gupta, V.S. Chauhan, N. Sankararamakrishnan, Water Res. 43 (2009) 3862.
[49] D.D. Gang, B. Deng, L. Lin, J. Hazard. Mater. 182 (2010) 156.

[50] C. Liu, B. Wang, Y. Deng, B. Cui, J. Wang, W. Chen, S.y. He, J. Nanomater. 2015 (2015) 191829.
[51] N. Qin, Y. Zhang, H. Zhou, Z. Geng, G. Liu, Y. Zhang, H. Zhao, G. Wang, J. Colloid Interface Sci. 472 (2016) 8.
[52] M.A.V. Ramos, W. Yan, X.q. Li, B.E. Koel, W.X. Zhang, J. Phys. Chem. C 113 (2009) 14591.
[53] S.R. Kanel, B. Manning, L. Charlet, H. Choi, Environ. Sci. Technol. 39 (2005) 1291.
[54] T. Phenrat, T.C. Long, G.V. Lowry, B. Veronesi, Environ. Sci. Technol. 43 (2008) 195.
[55] C. Wang, H. Luo, Z. Zhang, Y. Wu, J. Zhang, S. Chen, J. Hazard. Mater. 268 (2014) 124.